Path integral Monte Carlo study of SF_6-doped helium clusters

Yongkyung Kwon[a)]
Department of Chemistry, University of California, Berkeley, California 94720

David M. Ceperley
Department of Physics and National Center for Supercomputing Applications, University of Illinois, Urbana, Illinois 61801

K. Birgitta Whaley
Department of Chemistry, University of California, Berkeley, California 94720

(Received 14 August 1995; accepted 27 October 1995)

The path-integral Monte Carlo technique is applied to study the SF_6He_{39} cluster at low temperatures. The method employs as input only pair potentials, the number of atoms, and the temperature, and is thus independent of the trial function bias which can affect calculation of structural quantities in variational and diffusion Monte Carlo. We thereby obtain an unambiguous answer to the question of the location of SF_6 in small clusters (39 He atoms), as well as the temperature dependence of the cluster structure. The cluster is found to undergo a gradual transition to a superfluid between 0.625 K and 1.25 K, and to evaporate significantly at temperatures above 2 K. We also calculate spectral shifts for the ν_3 vibrational mode of SF_6, using the instantaneous dipole-induced dipole mechanism. The results are compared with infra-red absorption measurements and with the previous ground-state quantum Monte Carlo calculations. © *1996 American Institute of Physics.* [S0021-9606(96)02205-8]

I. INTRODUCTION

The study of helium clusters has attracted a great deal of interest among both theorists and experimentalists because of their unique finite-size quantum-liquid nature.[1] Furthermore, theory predicts that pure helium clusters ^4He_N would be superfluid at low temperatures.[2,3] Recent experiments on these clusters with atomic and molecular impurities attached have made it possible to conduct indirect probes of their structures. A basic question is the location of the impurity, which can depend on the competing effects of impurity-He binding energy, cluster size and temperature. Zero-temperature quantum Monte Carlo calculations for molecular impurities with a wide range of binding energies to helium have shown that as the impurity-helium potential increases, the molecule becomes more localized about the cluster center, and that for a given impurity, the molecular delocalization then increases as the cluster size increases.[4–6] However for boson quantum clusters such as helium, there may be an important distinction between the ground-state ($T=0$) structure and that for finite temperatures. At finite T below the superfluid transition temperature, injection of an impurity into helium may cause a free energy increase from loss of Bose permutation symmetry.[7] At $T=0$, Bose and Boltzmann statistics are identical and this free energy increase is absent. In a finite cluster, the extent of reduction in the Bose permutation symmetry of helium atoms surrounding the impurity can in principle be reduced if the molecule is situated near a surface or is only partially solvated. Since the free energy increase for complete loss of permutation symmetry of a helium atom in bulk is ~ 1 K,[7] this is an additional factor affecting the delicate energetic balance in weakly bound dopant-helium cluster systems.

In this paper we investigate the effect of finite temperature on the structure of SF_6He_N. Several infrared spectroscopic studies have been made on SF_6-doped helium clusters.[8–10] The vibrational spectrum shows an extremely narrow, red-shifted ν_3 absorption at $\omega=946.3\pm0.1$ cm^{-1} (FWHM $<$ 0.01 cm^{-1}), with two satellite bands.[9] High resolution analysis of these bands has enabled the spectrum to be fit to a model of a freely rotating spherical top, with rotational constant one third that of free SF_6.[10] Both spectroscopic[9,10] and mass spectrometric measurements[11] indicate that the SF_6 impurity is fully solvated and is located inside the cluster. This is not surprising, since SF_6 is strongly bound to helium and would be expected from chemical considerations to be completely solvated inside a cluster of He_N. Experimentally, the temperature of the cluster is measured as 0.4 ± 0.05 K.[10]

Several zero-temperature quantum Monte Carlo studies have been made for SF_6He_N.[4,12,13] While the most recent study[13] has confirmed the original prediction of a centrally located, quite well localized SF_6,[4] these calculations have indicated that analysis of ground-state structure by variational Monte Carlo (VMC) and diffusion Monte Carlo (DMC) can be complicated by long convergence times for impurity structural quantities and by trial wave-function bias. This stimulated us to employ the path-integral Monte Carlo (PIMC) method,[14] which is independent of any variational *ansatz*. The PIMC method also necessarily results in finite-temperature properties, and so enables us to examine whether the impurity exchange energy can play any significant role in affecting the location of the SF_6 within the clus-

[a)]Permanent address: Department of Physics, Kon-Kuk University, Seoul 133-701, Korea.

ter. At very low temperatures the PIMC results can be extrapolated to $T=0$K to compare with the ground-state properties.

II. THEORETICAL APPROACH

The path-integral Monte Carlo is a numerically accurate method to calculate thermodynamic properties of a quantum system, based on Feynman's original idea of mapping path integrals onto interacting classical *ring-polymers.* To date, the PIMC method incorporating quantum statistical exchange effects has been successfully applied to bulk liquid helium,[15,16] two-dimensional helium on hydrogen surfaces,[17] clusters of pure helium[2] and of *para*-hydrogen molecules.[18] A detailed review of the method and of bulk helium results is given by Ceperley.[7] We start from the many-body density matrix at a temperature T:

$$\rho(R,R';\beta)\equiv\langle R|e^{-\beta H}|R'\rangle, \tag{1}$$

where $\beta=1/k_BT$, H is the Hamiltonian of an N-body system, and R represents a $3N$-dimensional vector, $R\equiv\{\vec{r}_1,\vec{r}_2,\ldots\vec{r}_N\}$. Then the thermal average of an operator $\hat{O}$ is given by

$$\langle\hat{O}\rangle=Z^{-1}\int dRdR'\langle R'|\hat{O}|R\rangle\rho(R,R';\beta), \tag{2}$$

where $Z=\int dR\rho(R,R;\beta)$ is the partition function. Since we do not know the density matrix at low temperatures T, where our system is highly quantum-mechanical, it is replaced with a product of M higher-temperature density matrices at MT:

$$\rho(R,R';\beta)=\int\cdots\int dR_1dR_2\cdots dR_{M-1}\rho(R,R_1;\tau)\times\rho(R_1,R_2;\tau)\cdots\rho(R_{M-1},R';\tau), \tag{3}$$

where $\tau=\beta/M$. The pair product high-temperature density matrix at $\tau^{-1}=40$ K, which was shown to be accurate enough for bulk liquid He in Ref. 15, is used in this study of SF_6He_N clusters. For a Bose system, the density matrix should be symmetrized by summing over all permutations P of particle labels:

$$\rho_B(R,R';\beta)=\frac{1}{N!}\sum_P\rho(R,PR';\beta). \tag{4}$$

In order to calculate the multidimensional integral of Eq. (2) coupled with Eqs. (3) and (4), we employ a generalized Metropolis algorithm whose details can be found in Ref. 7. Both permutations P and paths $\{R,R_1,R_2,\ldots,R_{M-1},PR'\}$ are sampled with probability density proportional to $\rho(R,R_1;\tau)\rho(R_1,R_2;\tau)\cdots\rho(R_{M-1},PR';\tau)$. Then, the average of an operator $\hat{O}$ can be determined just by taking the average of $\langle R'|\hat{O}|R\rangle$ over the paths sampled:

$$\langle\hat{O}\rangle\approx\frac{1}{N_p}\sum_{\alpha=1}^{N_p}\langle R'^{(\alpha)}|\hat{O}|R^{(\alpha)}\rangle, \tag{5}$$

where N_p is the number of the paths sampled in the Monte Carlo process.

In treating the SF_6He_N clusters, we fix the SF_6 molecule at the origin for simplicity as is done in some of the ground-state calculations, i.e., we give it infinite mass. This is a reasonable approximation because its mass is much heavier than that of a helium atom. It results in a slight lowering of the zero-point energy relative to finite-mass SF_6 in He_N, but in very little change in structural features.[13] Thus the main contribution to any apparent delocalization of SF_6 in the cluster will arise from the delocalization of the He distribution about the heavier SF_6, and can be quantified by the He center-of-mass distribution about the stationary SF_6. For the potential energy, we use a sum of pair potentials between helium atoms and between SF_6 and He. Therefore, we have the following system Hamiltonian:

$$H=-\frac{\hbar^2}{2m}\sum_{i=1}^{N}\nabla_i^2+\sum_{i<j}V_{\mathrm{He-He}}(r_{ij})+\sum_{i=1}^{N}V_{\mathrm{He-SF_6}}(r_i), \tag{6}$$

where m is the mass of a helium atom, $r_{ij}=|\vec{r}_i-\vec{r}_j|$, and $V_{\mathrm{He-He}}$ ($V_{\mathrm{He-SF_6}}$) is the He–He (He–SF_6) interaction potential. This represents N helium atoms moving in an external field provided by the stationary SF_6. The widely used form of Aziz *et al.*[19] is employed for $V_{\mathrm{He-He}}$, while for the He–SF_6 interaction we use an isotropic version of the two-body potential proposed by Pack *et al.*[20] These are the same potentials as used in the previous ground-state calculations. According to Barnett and Whaley (BW),[4] incorporation of the anisotropy in $V_{\mathrm{He-SF_6}}$ has only a small ($<0.5\%$) energetic effect and does not influence the angle-averaged radial dependence of structural properties. Both interactions are short-ranged; the He–SF_6 interaction has well depth of 62 K, a factor of $\sim$6 times that of the He–He interaction. For the purpose of using a tabularized form of the density matrix,[15] we truncate the potentials smoothly at a certain distance as follows:

$$V(r)\rightarrow\begin{cases}V(r)-V(r_c) & \text{for } r<r_c\\ 0 & \text{otherwise}\end{cases}. \tag{7}$$

The cutoff radii are set to be 9 Å for the He–He interaction and 15 Å for the He–SF_6 interaction, yielding $V_{\mathrm{He-He}}(r_c)=-0.020$ K and $V_{\mathrm{He-SF_6}}(r_c)=-0.025$ K. The potential displacements caused by these values of $V(r_c)$ with Eq. (7) are negligible relative to the strength of the potentials in the interaction regime. We have not added any artificial confinement potential to prevent the helium atoms from evaporating, in contrast to Refs. 2 and 18. The stronger binding to the SF_6 molecule lowers the evaporation rate enough to make this feasible.

III. RESULTS

We have done path-integral calculations for the SF_6He_{39} cluster at $T=0.625$ K and 1.25 K. Calculations at higher temperatures showed increasingly large amounts of evaporation, discussed in more detail below. The $N=39$ cluster was chosen since this was the first size at which the issue of trial function bias became important in the $T=0$

TABLE I. The total energy of SF_6He_N calculated at $T=0.625$ K and 1.25 K using the PIMC method, together with the VMC and DMC ground-state energies (Ref 13). PIMC and A are for $N=39$, while B is for $N=40$. All energies are in units of K per helium atom. For $T=0.625$ K, $M=64$, and for $T=1.25$ K, $M=32$. SF_6 has infinite mass in all three calculations.

		A	B
VMC		−15.60(1)	−17.21(1)
DMC		−19.45(4)	−19.45(1)
PIMC	$T=0.625$ K	−19.40(4)	
	$T=1.250$ K	−18.89(5)	

calculations[12,13] and it is computationally still manageable with PIMC. Employing the high-temperature density matrices at $\tau^{-1}=40$ K gives $M=64$ and 32 path-integral partitions for $T=0.625$ K and 1.25 K, respectively.

We first calculate the cluster thermal average energy at these temperatures, and compare with the ground-state energies calculated by McMahon *et al.*[13] with two different trial functions, A and B (Table I). The trial function B was first proposed by Chin and Krotscheck (CK)[12] and then reoptimized by McMahon *et al.*,[13] while A is the same wave function as BW[4] used in their ground-state calculations. These differ primarily in the presence of a term inducing the peak structure of the He density distribution in B, which is absent in A. This term significantly improves the energy and structural properties at the VMC level (see Table I). Detailed discussion and comparison of these and other trial functions are given in Ref. 13. Hereafter A and B represent the trial functions themselves or the ground-state results obtained with them in Ref. 13, for $N=39$ (A) and $N=40$ (B), respectively. Both these ground-state calculations were performed with the mass of SF_6 set to infinity, just like our PIMC calculation. The DMC energies for A and B, which are in principle independent of trial functions used, would be expected to differ because of different number of particles involved in these calculations. However, we see that the two energies are exactly the same in Table I. This reflects the possibility that one of these energies has been affected by the time step error in the DMC process.[13,21] Both DMC energies are lower than that at $T=1.25$ K, by $\sim$ 0.5 K per He, but are the same as that at $T=0.625$ K within statistical error. The total thermal energy increase from $T=0.625$ K to $T=1.25$ K is about 20 K, which is largely due to the presence of evaporated particles at the higher temperature. Note that the average energy at $T=1.25$ K includes the evaporated helium atoms. The discussion of energetics here has not considered the tail corrections due to the truncation of the potentials in Eq. (7).

We have also done the calculations without including permutational moves (no exchange effects). While the exclusion of exchange effects causes very little change in the total energy at $T=1.25$ K, it produces a significant energy increase at $T=0.625$ K, by about 0.37 K per helium atom. This is less than the value in bulk helium, which is about 1 K at this temperature.[7] The lower exchange energy loss in the cluster reflects only partial loss of Bose permutation symmetry induced by the pinning of some He to the SF_6 impurity,

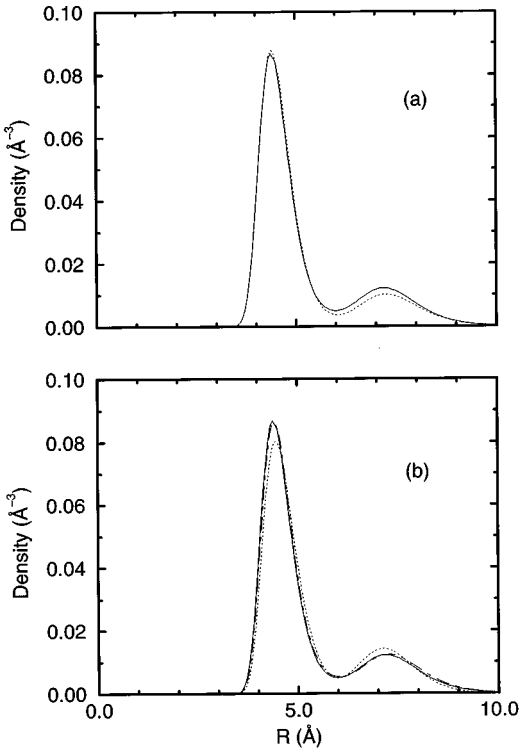

FIG. 1. The helium density profiles of SF_6He_N (a) at $T=0.625$ K (solid curve) and 1.25 K (dotted curve), and (b) at $T=0.625$ K (solid curve) and at $T=0$ K (dotted curve: A, dashed curve: B). The origin is set to be the position of SF_6. PIMC and A results are for $N=39$, while B is for $N=40$.

relative to the bulk. The importance of exchange effects at the lower temperature will be addressed again below.

Figure 1(a) shows the helium density distributions around SF_6 at $T=0.625$ K (solid curve) and 1.25 K (dotted curve). For the distributions at both temperatures, there is a shell structure peaked at $\sim$4.3 Å where the helium density is comparable to those of the solid at high pressures. The first shell includes about 23 helium atoms, which is consistent with the DMC calculations of BW.[4] According to their calculations, the first-shell structure hardly changes over a wide range of cluster sizes ($39 \leqslant N \leqslant 499$). Our calculations show that this solvation shell is not affected by a temperature increase up to 1.25 K. There is another peak in the helium density, located at about 7.2 Å from SF_6. This second peak is lower at $T=1.25$ K than either at $T=0.625$ K or at $T=0$ [see Fig. 1(b)], because at higher temperatures thermal motion tends to disperse the helium atoms beyond the first shell, which are more weakly bound to the SF_6. Furthermore, we have found that some helium atoms are evaporating during the path-integral run at 1.25 K. Typically one or two atoms are seen at distances $R>24$ Å from the SF_6. The evaporated particles account for the significant lowering of the second peak in Fig. 1(a) at the higher temperature. Additional calculations at $T=2.5$ K and 5.0 K show increased evaporation, to the extent that the cluster is completely evaporated by 5.0 K.

We compare in Fig. 1(b) the PIMC helium density profile for $T=0.625$ K with the ground-state densities obtained using trial functions A and B. The dotted line shows the A

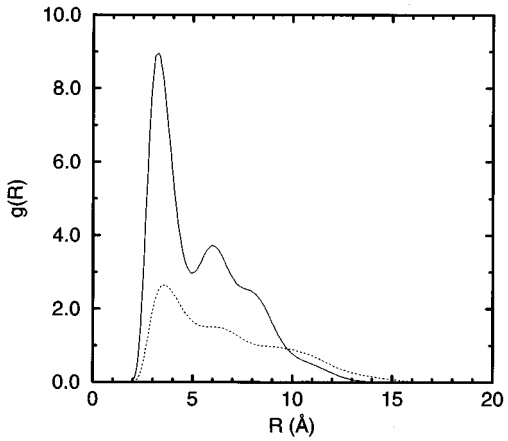

FIG. 2. The pair distribution functions $g(r)$ between the helium atoms in the first shell (solid curve) and between the second-shell atoms (dotted curve) of SF_6He_{39}. The calculation was done at $T=0.625$ K and the length unit is Å.

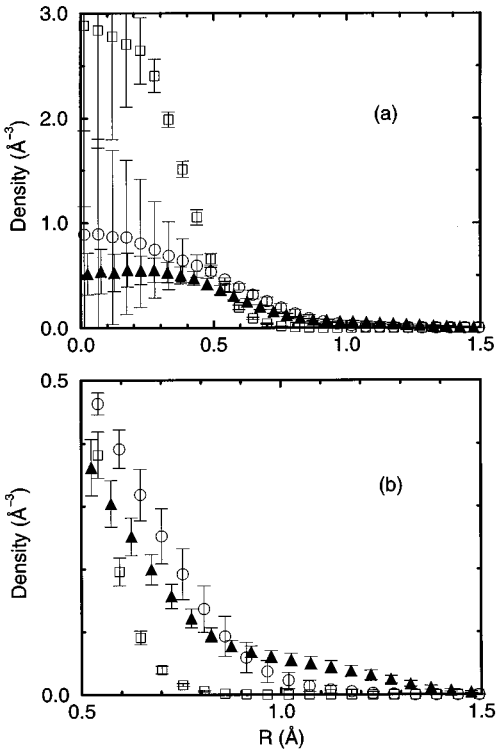

FIG. 3. The helium center-of-mass distribution in SF_6He_N with respect to SF_6 fixed at the origin. PIMC calculations at $T=0.625$ K (filled triangles); DMC ground-state calculations from Ref. 13 (A: open squares, B: open circles). (b) is just an enlargement of (a) at larger distances. PIMC and A results are for $N=39$, while B is for $N=40$.

($N=39$) helium distribution about SF_6, the dashed line the B ($N=40$) distribution, and the solid line represents our PIMC result for SF_6He_{39}. Since the importance-sampled DMC process gives rise to a set of random walks whose probability density is proportional to the product of trial function and the exact ground-state function, the accurate computation of a structural quantity which does not commute with the Hamiltonian requires an extrapolation from the VMC and DMC results.[22] This is the point at which the trial wave function bias can occur in DMC calculations of structural quantities. The two $T=0$ K results in Fig. 1(b) are the extrapolated ones, and lie between the corresponding VMC and DMC results. As can be seen, the result A has a significantly lower first peak and a little higher second peak than the others, while B and our PIMC result are very consistent with each other, except at large distances beyond the second peak. This difference at large distances is due to the additional particle in the B calculation ($N=40$). From this comparison, one can say that wave function B is more accurate than A as far as the helium density distribution is concerned. This confirms the improved representation achieved by the addition of peak structures in the trial wave function B.[12,13] It is also reflected in the lower VMC energy obtained for B (Table I), but the similarity of the structure with PIMC provides a more compelling argument. Similar improvement is achieved by other trial functions implicitly containing the He density structure, as is discussed by McMahon *et al.*[13]

Figure 2 shows pair distribution functions at $T=0.625$ K, calculated separately between helium atoms in the first shell and between the second-shell heliums. These functions are defined as follows:

$$g^{(i)}(r)=\frac{\Omega}{N^2}\left\langle \sum_m{}' \sum_{n\neq m}{}' \delta(\vec{r}-\vec{r}_{mn})\right\rangle, \tag{8}$$

where the primes mean that the summations are done only over the helium atoms in the ith shell. It is natural from Fig. 1 to choose the first-shell region as a sphere of radius 6 Å, and the second shell as the rest of the space. In order to obtain a finite normalization, we set Ω to be the volume of a cube with side 28 Å, which can be justified from the fact that no helium atom is likely to be further than 14 Å from the SF_6 at $T=0.625$ K (see Fig. 1). The first-shell pair distribution function, represented by the dotted curve, has a more structured form than the second-shell one represented by the dotted curve. This reflects the fact that the helium atoms in the first shell are more solid-like due to the strong interaction with the impurity molecule. Because of the finite size of the system, both distributions go to zero at large distances.

The helium center-of-mass distribution with respect to the impurity molecule (or equivalently the impurity distribution with respect to the center of mass) at $T=0.625$ K is shown in Fig. 3, along with the DMC extrapolated results (A and B) obtained by McMahon *et al.*[13] For higher temperatures, the presence of even a few evaporated particles gives rise to an ambiguity in calculation of the center-of-mass distribution because the positions of those particles, which are irrelevant to the properties of the bound system, nevertheless dominate the determination of the center-of-mass location. Therefore we restrict the discussion here to the result for $T=0.625$ K and comparison with the $T=0$ calculations. Since Fig. 3 represents a probability density in three dimensions, it has much larger statistical fluctuations at small distances than at large distances. Unlike CK's original results for a trial function of type B,[12] the impurity distributions

from all three calculations do not have a peak clearly displaced from the center. Rather, its maximum density seems to be located at the center, just as in the ground-state calculations of BW.[4] McMahon *et al.*[13] concluded that CK's finding of the impurity being displaced from the center is due to the lack of the convergence in CK's DMC calculation.

Figure 3 (a) shows that our PIMC distribution at $T=0.625$ K has a much larger spread than the result A and is quite similar to B at short distances, even considering the large statistical errors. This confirms the previous conclusion made from Fig. 1, namely that the trial wave function B is structurally more accurate than A. Note that there is more difficulty in obtaining the statistically converged SF_6 distribution than the He distribution, because we get only one sample of the center-of-mass location from each configuration R, for every 39 samples of the He location. One can see in Fig. 3(b), which is an enlargement of Fig. 3(a) at distances of 0.5−1.5 Å, that beyond 1 Å the $T=0.625$ K distribution is higher than the distribution A. This higher probability at large distances could result from thermal broadening rather than the wavefunction bias in the DMC calculation. According to Krotscheck and Chin's variational estimates,[23] the *dipole excitation* energy is about 0.8 K for $N=39$, so it is possible that this quantized vibration mode could affect the PIMC calculation at $T=0.625$ K. Since this excitation accounts for relative oscillations between the helium center of mass and the impurity, its effect would be most noticeable in the center-of-mass distribution. It does not give much contribution to the $T=0.625$ K energy in Table I (where the energies are in units of K per particle), since an increase of 0.8 K in the *total* energy is within the statistical error of our calculation.

We also compute the spectral shifts of the SF_6 intramolecular vibrations, using the instantaneous dipole-induced dipole (IDID) mechanism originally proposed by Eichenauer and LeRoy[24] to calculate the vibrational spectra of SF_6 in classical simulations of SF_6-doped argon clusters. The same mechanism was used by BW for SF_6He_N in their ground-state calculations.[4] This approach is based on the assumption that the instantaneous dipole moment of SF_6 during the ν_3 vibrations induces dipole moments in the surrounding helium atoms, and that the resulting interactions between the SF_6 and He dipoles are the main cause of the spectral shifts. We define a spectral shift density for the ν_3 vibration by

$$P(\Delta\nu)=\frac{1}{3}\sum_{i=1}^{3}\langle\delta(\Delta\varepsilon_i(R)-\Delta\nu)\rangle, \tag{9}$$

where $\Delta\varepsilon_i(R)=\Delta E_{1_i}^{id}(R)-\Delta E_0^{id}(R)$, and $\Delta E_0^{id}(R)$ and $\Delta E_{1_i}^{id}(R)$ are the shifts of the ground and first excited vibrational state of SF_6 in the cluster configuration R. The detailed expressions for these quantities within the IDID model are given in Eqs. (18) and (19) of Ref. 24. In our finite temperature calculations, $\langle\cdots\rangle$ is computed by taking the average of the argument $\cdots$ over configurations sampled with probability density proportional to the diagonal density matrix $\rho_B(R,R;\beta)$, as in Eq. (5). In the zero-temperature DMC calculations, the probability density was taken to be the mixed distribution, which approximates the ground state density. When the zero- and low-temperature distributions are similar, as is implied by the similarities between the He and SF_6 distributions (Figures 1 and 3, respectively), this can be viewed as generating a pseudo-thermal distribution. The mixed estimator for $P(\Delta\nu)$ is then extrapolated according to the usual second order scheme.[4,22] The average spectral shift, $\Delta\nu_3$, is then given by

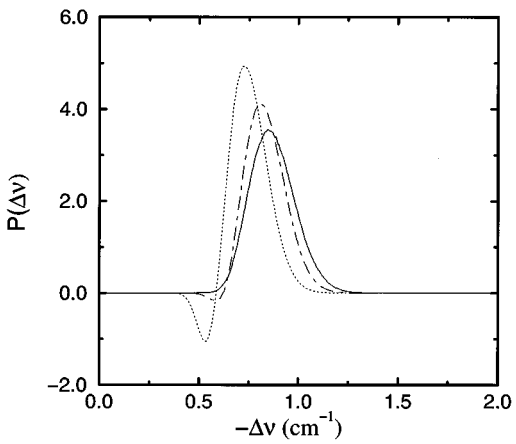

FIG. 4. The ν_3 spectral shift densities $P(\Delta\nu)$, defined by Eq. (9), for SF_6He_N, computed using the instantaneous dipole-induced dipole mechanism (Ref. 24). The solid line represents the PIMC result at $T=0.625$ K (solid line), while the dotted and dashed lines show the DMC ($T=0$) extrapolated results obtained from trial functions A and B, respectively. Frequencies are given in cm^{-1}. PIMC and A results are for $N=39$, while B is for $N=40$.

$$\Delta\nu_3=\int P(\Delta\nu)\Delta\nu d(\Delta\nu), \tag{10}$$

$$=\frac{1}{Z}\sum_m e^{-\beta E_m}\frac{1}{3}\sum_{i=1}^{3}\Delta\varepsilon_i^{(m)}, \tag{11}$$

$$=\frac{1}{Z}\sum_m e^{-\beta E_m}\Delta\varepsilon^{(m)}, \tag{12}$$

where $\Delta\varepsilon_i^{(m)}=\langle\Psi_m|\Delta\varepsilon_i(R)|\Psi_m\rangle$ is the expectation value of $\Delta\varepsilon_i(R)$ in the cluster state Ψ_m, and $\Delta\varepsilon^{(m)}$ is the resulting average spectral shift of the three SF_6 ν_3 vibrations in state m.

Figure 4 shows the ν_3 spectral shift densities, $P(\Delta\nu)$, for SF_6He_{39} calculated at $T=0.625$ K (solid line), together with the extrapolated DMC results obtained from trial functions A and B, using the parameters and algorithm of Ref. 13 (dotted and dashed lines, respectively). The general similarity between the zero and finite T results derives from the similarity of the He density distributions in the region of the first solvation shell, the second shell being located at distances too large to contribute much to the spectral shift. Differences between the three spectral shift density distributions arise from the small quantitative differences in He and SF_6 density distributions, the closer similarity of the lineshift B to the PIMC shift reflecting the improved structural representation of the B versus A trial functions. These differences are

most evident near $\Delta\nu\sim-0.5$ cm^{-1}, where trial function A is seen to result in appreciable negative spectral shift density after the usual second order extrapolation is made. These non-physical negative values reflect a large difference between the VMC and DMC mixed spectral shift densities, and are clearly less significant for the $T=0$ shift density derived from trial function B (dashed line). The latter also lies closer to the finite temperature path integral result. The average shift at $T=0.625$ K is $\Delta\nu_3=-0.84$ cm^{-1}, and the extrapolated shift at $T=0$ from trial function A is $\Delta\nu_3=-0.73$ cm^{-1}, while that from trial function B is $\Delta\nu_3=-0.81$ cm^{-1}. (BW obtained a $T=0$ value of -0.82 cm^{-1} using a third trial function of similar quality to B in terms of structural and energetic accuracy.[4]) These average shifts are negative, indicating a red-shift from the gas-phase ν_3 frequency, and show negligible effect of temperature over the range $T=0-0.625$ K. However, the magnitude of the shifts in all calculations is noticeably smaller than the experimental shift of -1.6 cm^{-1} found in Refs. 8 and 9.

In previous work,[4,24] spectral shift density distributions calculated according to Eq. (9) were equated with a heterogeneous line shape profile for the $\Delta\nu_3$ absorption. (The homogeneous lifetime broadened width cannot be obtained from the IDID mechanism because the quadratic IDID terms in the potential expansion do not cause transitions out of the triply degenerate first excited ν_3 vibrational state of SF_6.) Figure 4 confirms that the $T=0$ distribution can indeed be used as a good approximation to the low temperature spectral density distribution, as was assumed in Ref. 4. However, this similarity also implies that few excited states contribute at $T=0.625$ K, and that there should therefore be little contribution from heterogeneous broadening. This has two implications. First, it is therefore likely that the experimental linewidths are merely lifetime-broadened. Theoretical analysis of this in terms of vibrational energy transfer requires knowledge of terms of odd order in the SF_6 internal stretching dependence of the SF_6–He interaction potential. These are currently unknown. Second, the identification of Eq. (9) with a heterogeneous lineshape is not generally valid in quantum mechanics, and becomes particularly problematic at low temperatures when few states contribute. This is apparent upon constructing an alternative spectral shift density $P'(\Delta\nu)$ directly from the operational definition of a heterogeneous lineshape deriving from thermal population of states,

$$P'(\Delta\nu)=\frac{1}{Z}\sum_m e^{-\beta E_m}\frac{1}{3}\sum_{i=1}^{3}\delta(\Delta\varepsilon_i^{(m)}-\Delta\nu). \tag{13}$$

Integrating $\Delta\nu$ over $P'(\Delta\nu)$ yields the same average shift $\Delta\nu_3$ as does $P(\Delta\nu)$, but only $P'(\Delta\nu)$ yields the correct limit of the heterogeneous line shape profile at $T=0$, i.e., a sum of three delta functions. The difference lies in the location of the delta function, which is immaterial only when the full average over $P(\Delta\nu)$ to obtain $\Delta\nu_3$ is performed. Thus it is important to bear in mind that spectral shift densities are not unique, and are not necessarily a measure of the heterogeneous line shape. Eq. (13) is not amenable to a path integral calculation, so the only estimate of the heterogeneous linewidth we can give is therefore derived from the $T=0$ calculations. These show that $\Delta\varepsilon^{(0)}$ is not split, i.e., the three-fold degeneracy of the ν_3 mode is retained when SF_6 is solvated by He_{39} in its ground state.[4] Therefore the heterogeneous broadening is zero at $T=0$. This is not surprising, given the high symmetry of the He density about the SF_6 in the non-rotating ground state.

The shortcomings of the IDID model lie in the assumptions that only the vibrational dependence of the long range interaction is significant, and that this may be approximated by an electrostatic model. While this was valid for SF_6 in Ar_N,[24] the polarizability of He is much less than that of Ar, so that the long range terms are much weaker. The contribution from the repulsive part is unknown and has been ignored. A more detailed investigation of the intramolecular vibrational dependence of the SF_6–He interaction would be very desirable for analysis of the homogeneous linewidth. Another desirable extension from the spectroscopic perspective is to explicitly incorporate the SF_6 rotational and vibrational degrees of freedom in PIMC and DMC calculations. The mere inclusion of potential anisotropy was shown by BW[4] to have negligible effect on the lineshape, although it did cause some resolution of angular structure in the first peak of the He density distribution. Explicit incorporation of the rotational wavefunctions of SF_6 could more drastically affect the sampling of the potential, and would be desirable in more detailed studies of the spectroscopy.

One of the most interesting properties of the helium clusters is their superfluid behavior. According to Pollock and Ceperley,[15] the probability that a particle is engaged in a permutation cycle involving several particles can be used to determine the degree of superfluidity, at least qualitatively. This was previously used to study the extent of superfluidity in clusters of pure helium and of *para*-hydrogen molecules by Sindzingre *et al.*[2,18] Fig. 5 shows snapshots of typical Feynman paths projected onto the XY plane at (a) $T=0.625$ K and (b) $T=1.25$ K. Since the timeslice $\tau=1/40$ K^{-1} has been used throughout these calculations, a path of a single helium atom consists of 64 timeslices at $T=0.625$ K and 32 timeslices at $T=1.25$ K. The thick solid lines in Fig. 5(a) represent a permutation cycle involving 15 helium atoms, and the thick dotted lines show cycles involving three atoms. Each closed polymer consisting of thin lines corresponds to a path of a single atom which does not participate in a permutation move. The SF_6 is represented by a single point at the origin. At $T=1.25$ K, we do not see any long paths involving several permuting atoms, while permutation moves or exchange effects are seen to be quite important at the lower temperature. The existence of these long permutations suggests that the SF_6He_{39} cluster may show more superfluid behavior as the temperature is lowered between 0.625 K and 1.25 K. In order to study this phenomenon quantitatively, we have computed the superfluid fraction in the helium density by calculating the moment of inertia of the system and comparing with that of the corresponding classical system. The details of this process are explained in Ref. 7. We have found that the superfluid frac-

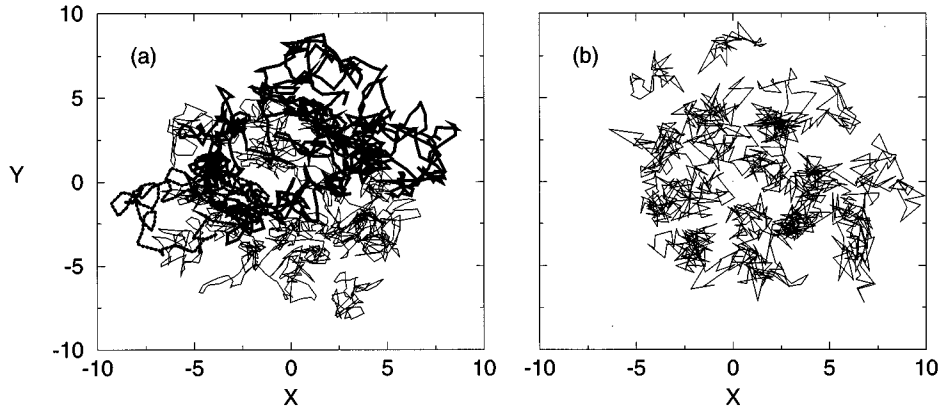

FIG. 5. Snapshots of the paths in the PIMC runs projected onto the XY-plane at (a) $T=0.625$ K and (b) $T=1.25$ K, for SF_6He_{39}. The thick solid lines represent a permutation cycle involving 15 helium atoms and the thick dotted lines show one involving three atoms. Each closed polymer consisting of thin lines corresponds to a path of a helium atom which does not participate in a permutation move. The SF_6 molecule is fixed at the origin and is therefore represented by a single point at (0,0). The length unit used is Å.

tion ρ_s/ρ of the SF_6He_{39} cluster is 0.67(7) at $T=0.625$ K, and 0.05(1) at $T=1.25$ K. The PIMC calculation of Sindzingre *et al.*[2] for pure helium clusters showed that ρ_s/ρ of an $N=64$ cluster is 0.9(1) at $T=0.625$ K, and 0.6(1) at $T=1.25$ K. The difference between the results for doped and for pure clusters is mainly due to the fact that the SF_6 impurity strongly binds the surrounding helium atoms and thereby suppresses the superfluidity, since the neighboring atoms cannot fully participate in the global exchange. Thus the superfluid state occurs at a lower temperature than in pure He_N (Fig. 1 of Ref. 2). However the exchange is not completely suppressed in the first solvation shell, and we do see permutation moves causing exchanges between first- and second-shell He atoms in Fig. 5 (a), despite the very different structural features these show (Fig. 2). The smaller number of heliums in our calculation may also be a factor in the reduction of ρ_s/ρ; Sindzingre *et al.* showed that the superfluid density does decrease with smaller cluster size.

IV. CONCLUSIONS

In summary, we have performed PIMC calculations for the SF_6He_{39} cluster at low temperatures. PIMC has the advantage of giving results for structural quantities which are free of bias due to a trial function, unlike DMC calculations. Therefore it is extremely useful for analyzing dopant distributions, since the ground-state energy is relatively insensitive to small changes in this, even for strongly-bound dopants such as SF_6.

For SF_6He_{39}, assuming an infinite mass SF_6, the average energy at $T=0.625$ K is as low as the previously-reported ground-state energy[12,13] within statistical error. At this temperature, both He and SF_6 density profiles are consistent with the $T=0$ converged DMC results,[13] confirming the presence of a strongly bound first solvation shell with ~ 23 He atoms and a centrally located SF_6, confined within 1.5 Å of the cluster center of mass. Furthermore, the PIMC results for both He and SF_6 densities allow a distinction between energetically equivalent DMC calculations made with different trial function forms. In particular, it is found that trial functions tailored to reproduce the He density peaks in the first and second solvation shell at the VMC level, give DMC distributions closer to the PIMC results.

The SF_6He_{39} cluster is seen to be extremely sensitive to temperature. The thermal energy increases by ~ 20 K on raising the temperature from $T=0.625$ K to $T=1.25$ K, which is accompanied by evaporation of several He atoms from the outer shell. Further raising of the temperature increases the extent of evaporation, with the entire cluster being evaporated by 5 K. There is a marked energetic contribution of the exchange permutation symmetry at $T=0.625$ K, about 0.37 K per He atom, which results from the partial loss of Bose permutation symmetry induced by some extent of pinning of He to the impurity. However there is no evidence that the SF_6 is preferentially located near the surface in order to minimize its number of nearest neighbors, as a result of this. The strength of the SF_6–He interaction clearly outweighs this finite-temperature Bose characteristic. A more weakly bound impurity, such as Ne, is therefore required to see the impurity location affected by the exchange symmetry energetics.[25]

Evaluation of the finite-temperature spectrum of the SF_6 ν_3 vibrational mode within the IDID model of Eichenauer and LeRoy gives a lineshift equal to $\sim 1/2$ of the experimental red shift of -1.6 cm^{-1}, while the close similarity of the finite T spectral shift densities with the corresponding $T=0$ densities suggests that the heterogeneous linewidth is negligible at $T=0.625$ K, just as it is zero at $T=0$. A more detailed knowledge of the internal molecular stretching dependence of the SF_6–He interaction is required in order to analyse the homogeneous linewidth, which we conclude is responsible for the small experimental broadening. It would also be useful to investigate the effect of the SF SF_6 rotational motion directly in a PIMC calculation.

One of the most interesting conclusions of these calculations is the existence of a significant superfluid fraction at $T=0.625$ K. At $T=1.25$ K there is essentially no exchange

contribution to the energy and there are also no long permutation cycles. The gradual transition to a superfluid therefore appears to be depressed to somewhere between $T=1.25$ K and $T=0.625$ K, considerably lower than that in pure He clusters.[2] Nonetheless, at $T=0.625$ K, the superfluid fraction is still 0.67(7), relative to 0.9(1) for pure He_N with $N=64$. This appears large, considering both the small size ($N=39$) of our cluster and the strong binding to, and localization about, the SF_6 impurity. Furthermore, not only the weakly bound, second solvation shell He atoms but also the strongly bound, first solvation shell atoms participate in the long permutation cycles responsible for superfluidity. Thus it emerges that the first solvation shell is not locked into a rigid, solid-like role, despite the high degree of localization in the radial direction, and that these He atoms do still participate in quantum exchange. A challenging question for future study is now the relationship between this superfluid behavior, which appears resistant to the embedding of strongly bound dopant molecules, and the extremely narrow infrared vibrational linewidths of the dopants, which appear to be quite a general feature.[26]

ACKNOWLEDGMENTS

We would like to thank R. N. Barnett and M. A. McMahon for helpful discussions. This work has been supported by the Air Force Office of Scientific Research under grant AFOSR F04611-94-K-0032. Y. Kwon acknowledges partial support from Kon-Kuk University under its 1995 research grant. The calculations were performed on the C90 at San Diego Supercomputing Center, and on IBM RISC/6000 workstations at the Graphics Center of the Berkeley Chemistry Department supported by the National Institutes of Health through Grant No. NIH S10 RR05651-01.

[1] K. B. Whaley, Intern. Rev. Phys. Chem. **13**, 1 (1994).
[2] P. Sindzingre, M. L. Klein, and D. M. Ceperley, Phys. Rev. Lett. **63**, 1601 (1989).
[3] M. V. Rama Krishna and K. B. Whaley, Phys. Rev. Lett. **64**, 1126 (1990).
[4] R. N. Barnett and K. B. Whaley, J. Chem. Phys. **99**, 9730 (1993); *ibid.* **102**, 2290 (1995).
[5] R. N. Barnett and K. B. Whaley, Z. Phys. D **31**, 75 (1994).
[6] M. A. McMahon, R. N. Barnett, and K. B. Whaley, Z. Phys. B **98**, 421 (1995).
[7] D. M. Ceperley, Rev. Mod. Phys. **67**, 279 (1995).
[8] S. Goyal, D. L. Schutt, and G. Scoles, Phys. Rev. Lett. **69**, 933 (1992).
[9] R. Fröchtenicht, J. P. Toennies, and A. Vilesov, Chem. Phys. Lett. **229**, 1 (1994).
[10] M. Hartmann, R. E. Miller, J. P. Toennies, and A. Vilesov, Phys. Rev. Lett. **75**, 1566 (1995).
[11] A. Scheidemann, B. Schilling, and J. P. Toennies, J. Phys. Chem. **97**, 2128 (1993).
[12] S. A. Chin and E. Krotscheck, in *Recent Progress in Many-Body Theories*, edited by E. Schachinger *et al.* (Plenum, New York, 1995), Vol. 4, p. 85.
[13] M. A. McMahon, R. N. Barnett, and K. B. Whaley, J. Chem. Phys. (to be published).
[14] E. L. Pollock and D. M. Ceperley, Phys. Rev. B **30**, 2555 (1984); D. M. Ceperley and E. L. Pollock, Phys. Rev. Lett. **56**, 351 (1986).
[15] E. L. Pollock and D. M. Ceperley, Phys. Rev. B **36**, 8343 (1987).
[16] D. M. Ceperley and E. L. Pollock, Phys. Rev. B **39**, 2084 (1989).
[17] M. Wagner and D. M. Ceperley, J. Low Temp. Phys. **89**, 581 (1992).
[18] P. Sindzingre, D. M. Ceperley, and M. L. Klein, Phys. Rev. Lett. **67**, 1871 (1991).
[19] R. A. Aziz, F. R. W. McCourt, and C. C. K. Wong, Mol. Phys. **61**, 1487 (1987).
[20] R. T. Pack, E. Piper, G. A. Pfeffer, and J. P. Toennies, J. Chem. Phys. **80**, 4940 (1984).
[21] P. J. Reynolds, D. M. Ceperley, B. J. Alder, and J. W. A. Lester, J. Chem. Phys. **77**, 5593 (1982).
[22] D. M. Ceperley and M. H. Kalos, in *Monte Carlo Methods in Statistical Physics*, edited by K. Binder (Springer-Verlag, Berlin, 1986).
[23] E. Krotscheck and S. A. Chin, Chem. Phys. Lett. **227**, 143 (1994).
[24] D. Eichenauer and R. J. LeRoy, J. Chem. Phys. **88**, 2898 (1988).
[25] D. M. Ceperley, unpublished.
[26] M. Hartmann, R. E. Miller, J. P. Toennies, and A. Vilesov, submitted to Science.